Four-probe electrical-transport measurements on single indium tin oxide nanowires between 1.5 and 300 K

2009 Nanotechnology 20 105203

(http://iopscience.iop.org/0957-4484/20/10/105203)

Nanotechnology **20** (2009) 105203 (7pp) doi:10.1088/0957-4484/20/10/105203

Four-probe electrical-transport measurements on single indium tin oxide nanowires between 1.5 and 300 K

Shao-Pin Chiu[1], Hui-Fang Chung[2], Yong-Han Lin[3], Ji-Jung Kai[2], Fu-Rong Chen[2] and Juhn-Jong Lin[1,3]

[1] Institute of Physics, National Chiao Tung University, Hsinchu 30010, Taiwan
[2] Department of Engineering and System Science, National Tsing Hua University, Hsinchu 30013, Taiwan
[3] Department of Electrophysics, National Chiao Tung University, Hsinchu 30010, Taiwan

E-mail: jjlin@mail.nctu.edu.tw

Received 13 November 2008, in final form 31 December 2008
Published 16 February 2009
Online at stacks.iop.org/Nano/20/105203

Abstract

Single-crystalline indium tin oxide (ITO) nanowires (NWs) were grown by the standard thermal evaporation method. The as-grown NWs were typically 100–300 nm in diameter and a few μm long. Four-probe submicron Ti/Au electrodes on individual NWs were fabricated by the electron-beam lithography technique. The resistivities of several single NWs have been measured from 300 down to 1.5 K. The results indicate that the as-grown ITO NWs are metallic, but disordered. The overall temperature behavior of resistivity can be described by the Bloch–Grüneisen law plus a low-temperature correction due to the scattering of electrons off dynamic point defects. This observation suggests the existence of numerous dynamic point defects in as-grown ITO NWs.

(Some figures in this article are in colour only in the electronic version)

1. Introduction

In recent years, the science and technology of metal and semiconductor nanowires (NWs) have been very extensively explored [1, 2]. In addition to the material and application aspects, the fundamental physical properties of NWs have been investigated. The optical, magnetic and mechanical properties of NWs have drawn much theoretical and experimental attention. On the other hand, the electrical-transport properties of *individual* NWs have not been much studied. In fact, most electrical measurements on single NWs reported to date have mainly focused on either a two-probe configuration [3–5] or (in the case of semiconductor NWs) a field-effect-transistor configuration [6, 7]. Electrical-transport results obtained from *four-probe* measurements on single NWs over a wide range of temperature are still limited [8–11]. This lacking of four-probe results is probably partly due to the difficulties in fabricating good ohmic electronic contacts to individual NWs and partly due to the difficulties in handling and detecting nanoscale samples down to liquid-helium temperatures.

Among the numerous semiconducting and metallic NWs, Sn-doped In_2O_3 (indium tin oxide (ITO)) NWs have recently been studied [12–16]. Several groups have reported the growth behaviors and physical properties of ITO NWs. The interest in these nanoscale structures arises from the fact that the parent ITO material is a transparent conducting oxide. Moreover, the charge carriers in this material are established to be essentially free-electron-like. That is, the charge carriers behave like an ideal free electron gas with an effective mass of $m^* \approx 0.4\,m$ and a Fermi energy of $E_F \lesssim 1$ eV (whose value depends on the carrier concentration, n), where m is the free electron mass. The thermoelectric power (Seebeck coefficient) reveals a linear behavior from 300 K all the way down to liquid-helium temperatures, while the temperature behavior of resistivity is well described by the Bloch–Grüneisen law at not too low temperatures [17–19]. The carrier concentration in highly conductive ITO materials usually falls in the range from 10^{20} to 10^{21} cm^{-3} [20] and the room-temperature resistivity can be as low as $\sim$100 $\mu\Omega$ cm, if properly prepared [21].

In view of the nanoelectronic and optoelectronic applications, it is very useful to clarify whether the ITO

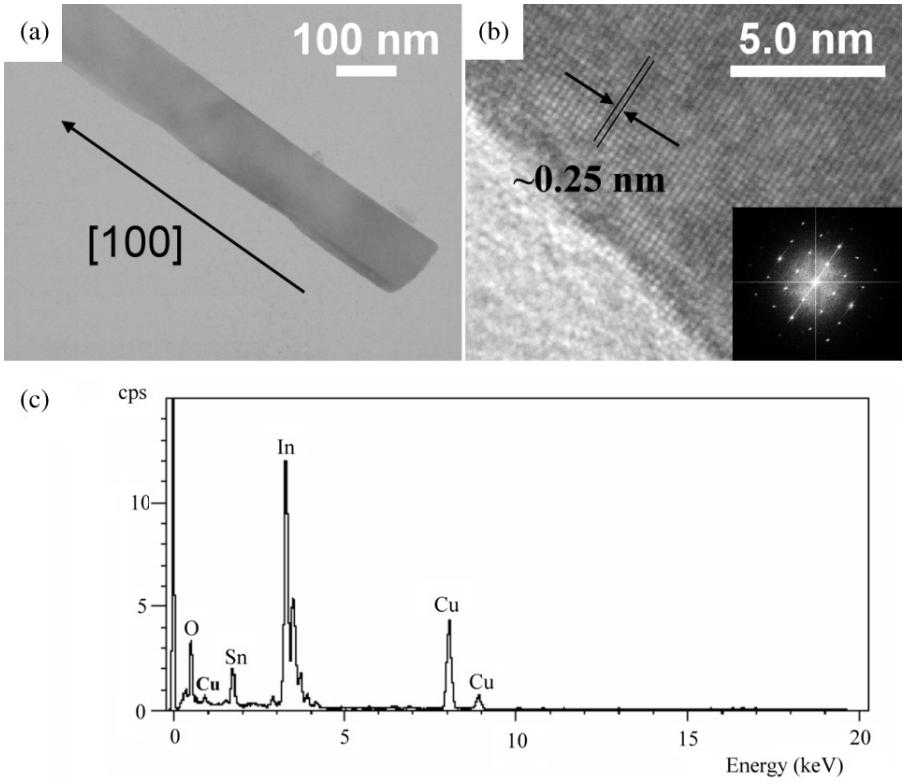

Figure 1. (a) A low magnification TEM image for a single ITO NW. (b) A high-resolution TEM image for the same ITO NW. The inset shows the corresponding selected-area electron diffraction pattern. (c) EDS spectrum for the ITO NWs grown on substrate A. The Cu peaks are due to the TEM Cu grids.

NWs still preserve the desirable electrical properties, such as metallic conduction and low resistivities. Thus far, there have been only a few reports on charge-transport measurements of single ITO NWs [16, 21, 22]. Besides, those measurements were performed on a two-probe configuration where the contributions from contact resistances and lithographic electrode resistances could not be excluded[4]. In this work, we present the first four-probe measurements on several single ITO NWs from 300 down to 1.5 K. These results thus represent the *intrinsic* electrical properties of individual single-crystalline ITO NWs.

2. Experimental method

ITO NWs were synthesized on 0.5 × 0.5 cm^2 Si substrates by the standard thermal evaporation method, as has been described previously [23]. Gold nanoparticles with a diameter of ∼20 nm were first dispersed on the Si substrates. Mixtures of indium (99.999% purity, Aldrich) and tin (99.9% purity, Merck) powders with a weight ratio of In:Sn = 9:1 were placed in the middle of a horizontal quartz tube. The spectrographic analysis as provided by the supplier indicated that the tin powders contained trace amounts of nonmagnetic (Bi: $\leqslant$ 0.01 at.%, Cu: $\leqslant$ 0.01 at.%, Pb: $\leqslant$ 0.05 at.%, Sb: $\leqslant$ 0.02 at.%) and magnetic (Fe: $\leqslant$ 0.02 at.%) impurities. A series of several Si substrates were placed near to the powders and were situated on the downstream side of the gas flow. An argon gas was input from one end of the quartz tube and the pumping speed at the other (downstream) end was adjusted to maintain an atmosphere of 50 Pa in the tube. The source powders were heated to 920 °C for 3 h, while the nearby Si substrate temperatures varied from ∼900 to ∼850 °C, depending on their distance to the source powders.

X-ray diffraction (XRD, MAC Science MXP-18) and high-resolution transmission electron microscopy (TEM, JEOL JEM-2010FX) studies indicated that the NWs were single crystalline, possessing a cubic bixbyite structure, and grew along the [100] direction. Figures 1(a) and (b) show a low magnification TEM image and an HRTEM image, respectively, for a single ITO NW. The morphology of the NWs was examined by field emission scanning electron microscopy (SEM, JEOL JSM-6330F). We found that the diameters, d, of the as-grown NWs were sensitive to the substrate temperature, and thus their sizes distributed widely among the substrates. The energy-dispersive x-ray spectroscopy (EDS, JOEL JEM-2010FX) and the inductively coupled plasma atomic emission spectrometry (ICP-OES, Perkin-Elmer Optima-3000DV) were utilized to determine the chemical compositions of the NWs. The former method determined the chemical compositions in a single NW, because the TEM electron beam was focused to a size of ≈3.7 nm, which was much smaller than the typical diameter of our NWs. The latter method determined the average chemical compositions by introducing a collection of

[4] In the case of metal NWs with good contacts, the two lithographic (e.g. Ti/Au or Cr/Au) electrode resistances may be of the same order of magnitude as the two contact resistances.

Table 1. Relevant parameters for four-probe individual ITO NW devices. T_s is the Si substrate temperature during the NW growth process. The character in parentheses following the temperature indicates the substrate name, A or B. Sn/In is the weight ratio of tin to indium. d is the NW diameter. ρ_{min} is the lowest measured resistivity of each sample. T_{min} is the temperature where ρ_{min} occurred.

Sample	T_s (°C)	Sn/In (wt%)	d (nm)	R (300 K) (Ω)	ρ(300 K) ($\mu\Omega$ cm)	ρ_{min} ($\mu\Omega$ cm)	T_{min} (K)	$\frac{\rho_{min}}{\rho(300\ K)}$
ITO-c-R	∼900 (A)	∼3.4	170	184.7	150	128	81	0.849
ITO-g	∼900 (A)	∼3.4	220	30.6	137	115	71	0.841
ITO-j1	∼850 (B)	∼5.3	110	476.2	215	190	87	0.881
ITO-11	∼850 (B)	∼5.3	130	286.2	293	263	88	0.896

many NWs into a chamber where the NWs were dissolved and ionized in an argon plasma. The compositions we obtained from these two complementary methods were consistent to within about 5%. We observed that the Sn content increased notably with decreasing Si substrate temperature. In the present study, we chose two substrates (referred to as A and B) with as-grown NWs for the fabrication of four-probe individual NW devices. The substrate temperature during the NW growth process was approximately 900 °C (850 °C) for substrate A (B). The weight ratio of Sn to In for the NWs was ∼3.4% for substrate A and ∼5.3% for substrate B. (For comparison, for those NWs grown on another Si substrate which was placed in between substrates A and B and having a substrate temperature of ∼880 °C during the growth process, we obtained an Sn/In weight ratio of ∼4.4%.) Figure 1(c) shows the EDS spectrum of the NWs grown on substrate A. It is clearly seen that Sn was effectively incorporated into the ITO NWs. Table 1 lists the values for the relevant parameters for the four NWs whose overall temperature behaviors of resistivity are studied in this work.

To fabricate four-probe individual NW devices for electrical-transport measurements, we first made micron-sized Ti/Au (10/60 nm) metal pads and coordinate marks by utilizing the standard photolithography and lift-off technique on Si substrates capped with a 400 nm thick SiO_2 layer. ITO NWs were then dispersed on the SiO_2/Si substrates. Individual NWs with diameters of ∼100–200 nm were identified and electrically connected to the pre-patterned micron-sized Ti/Au metal pads by using the standard electron-beam lithography and lift-off technique. In order to make good ohmic contacts to the NWs, an O_2 plasma was employed to clean the substrates before the Ti/Au (30/120 nm) electrodes contacting the NWs were deposited by the thermal evaporation method. The electrodes were typically a few hundreds of nanometers wide. An SEM image for a representative four-probe single ITO NW device is shown in the inset to figure 2.

The single NW devices were placed on a sample holder which was situated inside a dark vacuum can. The vacuum can was mounted on a standard ^{4}He cryostat for electrical resistance measurements from 300 down to 1.5 K. The four-probe current–voltage (I–V) characteristics were first checked by utilizing a Keithley K-6430 source meter as a current source and a K-182 nanovoltmeter. The I–V curves were linear even up to our maximum applied current of 1 μA. Figure 2 shows two representative I–V curves for the ITO-c-R NW at 297 and 4.2 K, respectively. An AC resistance bridge (Linear Research LR-700) was then employed for the

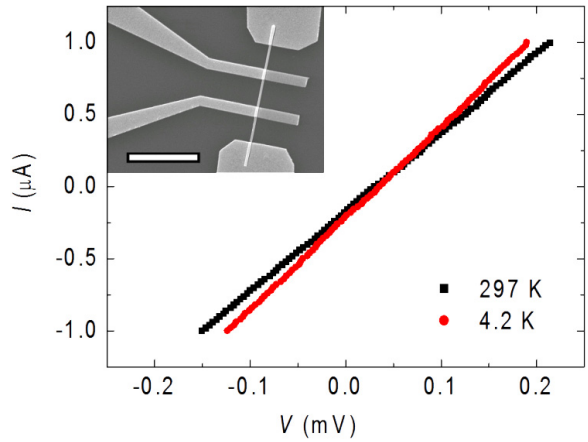

Figure 2. Current–voltage curves for the individual ITO-c-R NW at 297 and 4.2 K, as indicated. Notice that the I–V curves are linear. The inset shows an SEM image for this four-probe ITO NW device fabricated with electron-beam lithography. The scale bar is 5 μm.

measurement of temperature-dependent resistance, $R(T)$. It should be noted that, for all the results reported in this work, the values of $R(T)$ were determined with sufficiently small bias currents (typically, ∼30 nA) where the I–V characteristics were certainly linear and the electron heating effects were negligible down to our lowest measurement temperatures.

Inspection of table 1 indicates that the four-probe values of ρ(300 K) in the NWs taken from substrates A and B differ by roughly a factor of two. This amount of difference in resistivity should be considered satisfactory. The variation in resistivity from NW to NW may be accounted for by the variation of the Sn/In weight ratio as well as by the uncertainties in the individual NW dimensions which were needed to calculate the resistivity from the measured resistance. In fact, during the course of this study, we have also carried out *in situ* two-probe TEM–scanning tunneling microscopy (STM) measurements [24] on 17 single ITO NWs at room temperature and obtained an average resistivity of $\rho(300\ K) \approx 250 \pm 100\ \mu\Omega$. We point out that this resistivity value is several orders of magnitude lower than that in the ITO NWs grown by the electrospinning process [16]. For comparison, we also notice that recent experimental studies have reported that the resistivities of ITO NWs grown under nominally similar conditions could vary widely, from ∼100 $\mu\Omega$ cm to values higher than several thousands of $\mu\Omega$ cm [13, 21]. Then, the overall electrical quality of our as-grown ITO NWs should be considered as being relatively uniform and fairly good, i.e. our

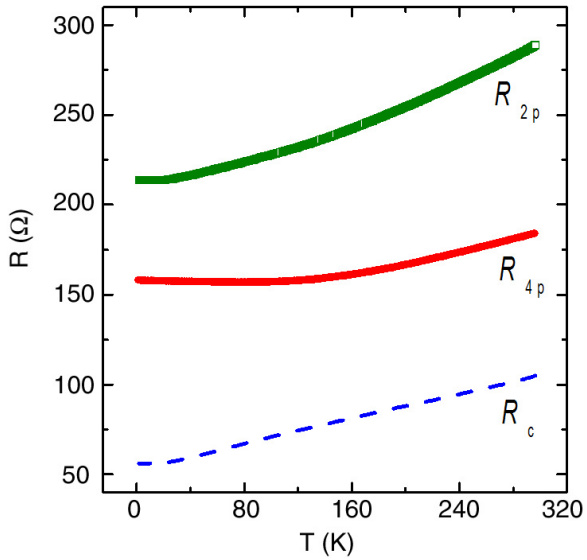

Figure 3. Measured two-probe, R_{2p}, and four-probe, R_{4p}, resistances as a function of temperature for the individual ITO-c-R NW devices, as indicated. The two-probe data were measured with the two inner electrodes as depicted in the inset to figure 2. The dashed line indicates the total contact resistance plus the lithographic electrode resistance, as given by $R_c(T) = R_{2p}(T) - R_{4p}(T)$.

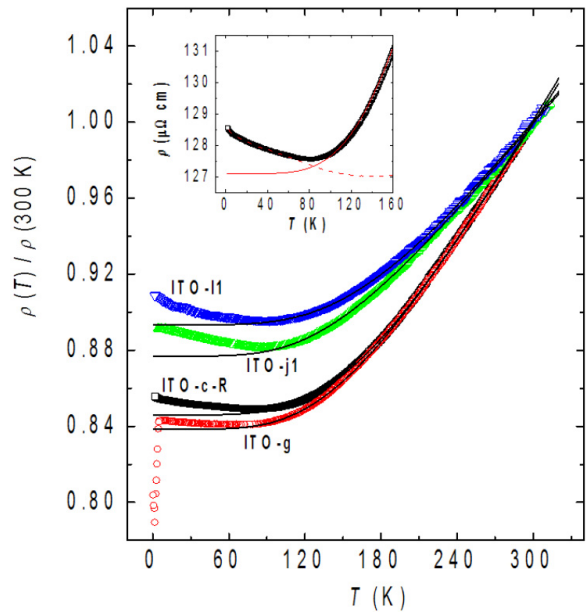

Figure 4. Normalized resistivities, $\rho(T)/\rho(300\ \mathrm{K})$, as a function of temperature for four individual ITO NWs, as indicated. The symbols are the experimental data and the solid curves are the theoretical predictions of equation (1). The inset shows the measured resistivity as described by the sum of the Bloch–Grüneisen law (solid curve) and a disorder-induced correction to ρ_0 (dashed curve) for the ITO-c-R NW.

resistivity values are approximately similar (to within a factor of ∼2–3) and comparatively low.

3. Results and discussion

Perhaps due to the experimental difficulties in fabricating lithographic contacting electrodes, the electrical resistances of single metal and semiconductor NWs reported in the literature were often measured by employing the two-probe method. However, it is well known that only the four-probe configuration can give the intrinsic resistances of the NWs under study [23]. Figure 3 shows the two-probe result and the four-probe result for the ITO-c-R NW whose SEM image was depicted in figure 2. Here $R_{2p}(T)$ denotes the resistance measured by employing the inner two electrodes as both the current and the voltage leads, while $R_{4p}(T)$ denotes the resistance measured by employing the outer two electrodes as the current leads and the inner two electrodes as the voltage leads. Obviously, the measured two-probe result includes not only the NW resistance but also the two contact resistances as well as the two lithographic Ti/Au electrode resistances. As a consequence, $R_{2p} > R_{4p}$ for all measurement temperatures. Moreover, the temperature behaviors of R_{2p} and R_{4p} are distinct. Thus, one should always be very cautious about drawing any conclusion from the results and analyses based on two-probe electrical-transport measurements[5].

The sum of the two contact resistances and the two lithographic electrode resistances can be quantitatively determined and is simply given by $R_c(T) \equiv R_{2p}(T) - R_{4p}(T)$ (the dashed line in figure 3). The smallness of the magnitude (<100 Ω) together with the metallic-like temperature behavior of R_c indicates that the two contacts are fairly good and ohmic. This observation demonstrates that low-resistance ohmic contacts can be readily achieved in nanoelectronic devices utilizing ITO NWs as interconnects. In the following, we shall concentrate on the four-probe results so as to address the intrinsic electrical resistivities of individual ITO NWs.

Figure 4 shows the four-probe results of the normalized resistivities, $\rho(T)/\rho(300\ \mathrm{K})$, as a function of temperature for four individual ITO NWs. We notice that the ITO-l1 and ITO-j1 NWs are more resistive than the ITO-c-R and ITO-g NWs, and hence the resistivity ratios $\rho(1.5\ \mathrm{K})/\rho(300\ \mathrm{K})$ are larger in the former NWs than in the latter NWs. (In the case of the ITO-g NW, we had compared the ratio $\rho(7\ \mathrm{K})/\rho(300\ \mathrm{K})$.) Nevertheless, in all four NWs, the resistivity ratios are close to unity, implying that the NWs must all contain large amounts of defects. That is, the residual resistivity is relatively high, as compared with the temperature-dependent phonon contribution. In the ITO-g NW, an unusual resistivity drop is seen at 5 K, which may signify a possible onset of superconductivity in this particular, i.e. our least resistive, NW [25, 26] (see below). Inspection of figure 4 suggests that our as-grown ITO NWs are metallic, namely their resistivities decrease with reducing temperature as the samples are cooled from 300 K down. Such temperature behavior of resistivity can be explained by the Bloch–Grüneisen law [27]:

$$\rho(T) = \rho_0 + \beta T \left(\frac{T}{\theta_D}\right)^4 \int_0^{\theta_D/T} \frac{x^5\,\mathrm{d}x}{(\mathrm{e}^x - 1)(1 - \mathrm{e}^{-x})}, \qquad (1)$$

[5] A comparison of two-probe and four-probe electrical-transport results for semiconductor ZnO NWs has recently been discussed in [11]. Discussions of the temperature behaviors of electronic contact resistances to metal NWs have been given in [9] and [23].

Table 2. Least-squares fitted (ρ_0, θ_D and β) and evaluated (l and $k_F l$) values of relevant parameters for individual ITO NWs.

Sample	ρ_0 ($\mu\Omega$ cm)	θ_D (K)	β ($\mu\Omega$ cm K^{-1})	l (nm)	$k_F l$
ITO-c-R	127	1047	0.571	10	30
ITO-g	115	958	0.492	11	33
ITO-j1	189	927	0.571	6.9	21
ITO-11	262	1086	0.802	5.0	15

where ρ_0 is a residual resistivity, β is an electron–phonon coupling constant and θ_D is the Debye temperature. Our experimental data for all NWs are least-squares fitted to the predictions of equation (1) (the solid curves) and the values of the fitted parameters (ρ_0, β and θ_D) are listed in table 2. Inspection of figure 4 clearly indicates that the experimental results can be well described by equation (1) at high temperatures of $T > T_{min}$, where T_{min} is defined as the temperature where the measured ρ assumes the minimum value, ρ_{min}. It is important to notice that our fitted values of β and θ_D are in good agreement with the corresponding values recently obtained in polycrystalline ITO films [17–19].

For the ITO materials with a room-temperature resistivity of ~200 $\mu\Omega$ cm, the Fermi energy is ≈0.9 eV [17]. Therefore, an estimate using the free electron model gives a value of the Fermi wavenumber $k_F \approx 3 \times 10^9$ m^{-1}. From the Drude resistivity $1/\rho = (ne^2\tau)/m^* = (k_F^2 e^2 l)/(3\pi^2\hbar)$, one obtains a value of the product $\rho l \approx 1.3 \times 10^{-14}$ Ω m^2, where e is the electron charge, $\hbar$ is Planck's constant divided by 2π and τ (l) is the electron elastic mean free time (path). Then, $l \approx 6.5$ nm and $k_F l \approx 20$. Notice that this value of l is much smaller than the diameter d of our NWs. Therefore, the NWs are three-dimensional with regard to the Bloch–Grüneisen transport.

At low temperatures of $T < T_{min}$, figure 4 indicates that the measured $\rho(T) > \rho_{min}$ and it slightly increases with reducing temperature. A plot of the variation of the normalized resistivity, $\rho(T)/\rho_{min}$, with $\sqrt{T}$ in figure 5 reveals that the low-temperature resistivity rise scales approximately with the square root of temperature in every NW. Except for the least resistive ITO-g NW, the amount of the resistivity rise is approximately 1%–1.5%. In particular, the amount of the resistivity rise basically increases with increasing ρ_{min}, suggesting that this $\sqrt{T}$ behavior must be closely associated with some sort of disorder effect. In other words, the disorder effect induces a temperature-dependent correction to the measured resistivity at low temperatures. The presence of high levels of disorder in our NWs is already shown from the fact that the resistivity ratios $\rho_{min}/\rho(300\text{ K})$ are close to unity in all of our NWs, see figure 4 and table 1. The nature of the randomness most likely reflects the existence of a great number of point defects in our as-grown ITO NWs, since our HRTEM studies indicated the absence of any linear and planar defects in the samples (while point defects could not be detected from the HRTEM study)[6]. In this regard, the four-probe electrical-transport measurements can be used as a very powerful probe for the microscopic quality of the atomic structure in a given NW.

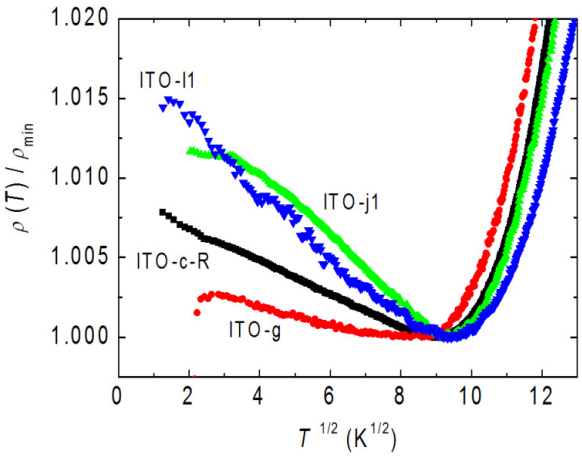

Figure 5. Normalized resistivities, $\rho(T)/\rho_{min}$, as a function of temperature for four individual ITO NWs, as indicated. Notice that the resistivity rises scale approximately with $\sqrt{T}$. For the ITO-j1 NW, there is a tendency to saturation below about 10 K, while for the ITO-g NW, there is an abrupt resistivity drop at 5 K.

In the presence of *static* defects in a normal metal, one may usually expect the quantum-interference weak-localization and electron–electron interaction effects to occur at low temperatures [29, 30]. These two effects lead to small, but explicit, temperature-dependent corrections to ρ_0 (or ρ_{min}). However, with the parameters pertinent to our samples (e.g. $k_F l \approx 20$, $D \approx 19$ cm^2 s^{-1} and $\rho \approx 200$ $\mu\Omega$ cm), we expect the two effects to cause a resistivity rise less than a tenth of a per cent down to 1.5 K. In other words, the resistivity rises that we observed in figure 5 (especially those in the ITO-j1 and ITO-l1 NWs) are more than one order of magnitude, as would be expected from the corrections due to the three-dimensional weak-localization and electron–electron interaction effects. Therefore, the two effects can only minutely be responsible for the observed resistivity rises[7].

Another kind of disorder effect that can lead to a low-temperature correction to resistivity originates from the scattering of electrons off *dynamic* structural defects. The dynamic defects can often be modeled as two-level tunneling systems, and the electron–dynamic defect scattering can be described in terms of the *nonmagnetic* two-channel Kondo effect. In this case, the resistivity correction is given by [31, 32]

$$\rho_{2CK}(T) = \frac{3n_i}{4\pi\hbar[eN(0)v_F]^2}\left[1 - 4\lambda\sqrt{\pi T}\right], \qquad (2)$$

[6] A similar result has recently been obtained in metallic single-crystalline RuO_2 NWs [28]. In that case, the HRTEM study also revealed a high-quality atomic structure, but the electron elastic mean free path l inferred from the four-probe electrical-transport measurements was only of the order of ~1 nm. Such a short mean free path implies strong scattering between conduction electrons and point defects.

[7] According to [22] and our preliminary measurements, the electron dephasing length $L_\varphi(T)$ in ITO NWs is shorter than a few tens of nanometers. Therefore, our NWs are three-dimensional (i.e. $d > L_\varphi$) with respect to the weak-localization effect. (Notice, however, that the L_φ was measured in a two-probe manner in [22]. Four-probe measurements should give a more accurate value.) Taking $D = 19$ cm^2 s^{-1}, the electron thermal diffusion length $L_T = \sqrt{D\hbar/k_B T} \approx (120/\sqrt{T})$ nm [29]. Thus, our NWs are also three-dimensional with regard to the electron–electron interaction effect over our measurement temperature range.

where n_i is the dynamic defect density, $N(0)$ is the electronic density of states per spin per channel at the Fermi level, v_F is the Fermi velocity and $\lambda \approx (T_{2CK})^{-1/2}$ is the coupling constant (T_{2CK} being the characteristic two-channel Kondo energy scale). Such a novel resistivity correction $\rho_{2CK} \propto \sqrt{T}$ has recently been realized in Co/(Cr/Ag)/Co trilayer systems [32] and perhaps also in a ThAsSe single crystal [33].

In the case of highly conductive ITO materials, it is known that the charge carriers can be very well described by a free-electron-like approximation [34, 35], as discussed in section 1. Therefore, the electronic density of states should take the form $N(0) \propto (m^*)^{3/2}(E_F)^{1/2}$ [36]. Since the effective electron mass $m^* \approx 0.4\,m$ and the Fermi energy $E_F \lesssim 1$ eV in ITO [17, 19], the value of $N(0)$ is approximately one order of magnitude smaller than that in a typical metal [26, 35]. Therefore, the resistivity correction ρ_{2CK}, which scales inversely with the square of $N(0)$, can be significantly larger in the ITO materials than in normal metals. (The value of $v_F = \hbar k_F/m^*$ in ITO is not much different from that in a typical metal.) Moreover, as discussed, the as-grown ITO NWs usually contain numerous point defects, and hence the dynamic defect concentration n_i in the samples can be relatively high[8]. Consequently, it is plausible to expect the ρ_{2CK} contribution to be important in these NWs. Thus, the $\sqrt{T}$ behavior observed in figure 5 may be reasonably ascribed to the novel nonmagnetic two-channel Kondo effect. Further studies in this direction can help to gain an insight into the microscopic properties and dynamics of the point defects in these NWs.

In the $T \to 0$ limit one may expect a breakdown of the scaling $\rho_{2CK} \propto \sqrt{T}$ due to interaction between two-level tunneling systems and a transition to the usual Fermi-liquid behavior, $\rho \propto T^2$, should occur [32]. This might be the case found in our ITO-j1 NW below about 10 K. This issue deserves further studies.

It is worth noting that the low-temperature resistivity rises which we observed in figure 5 cannot be ascribed to the standard (one-channel) Kondo effect originating from dilute magnetic impurities [37]. Our reasons are given as follows. (1) To the best of our knowledge, there have been no reports for the ITO materials being a magnetic Kondo system in the literature. (2) The resistivity rises in our NWs obey a $\sqrt{T}$ law, rather than the distinct $\ln T$ law as would be expected for the paradigmatic Kondo effect [37]. (3) Moreover, if our resistivity rises were to be attributed to the magnetic Kondo effect, a Kondo temperature of a few tens of kelvin would be required (recall that our $T_{min} \approx$ 70–90 K), which seems to be unrealistically high. (4) Finally, our magnetoresistance measurements indicated an extremely small magnetoresistance (see below), implying that magnetic impurities do not play a notable role in our samples. Therefore, we conclude that the standard magnetic (one-channel) Kondo effect cannot be responsible for the low-temperature resistivity rises which we found in figure 5.

Figure 6 shows the resistance as a function of temperature in zero magnetic field and in two perpendicular magnetic fields, as indicated, for the ITO-g NW below 12 K. (This part of the measurements was carried out with an Oxford Heliox ^{3}He fridge equipped with a 2 T superconducting magnet.) The magnetic fields were applied perpendicular to the direction of the current flow. Clearly, there is a resistance drop starting at 5 K in zero magnetic field. The resistance is partly restored in the presence of our applied magnetic fields, signifying that this resistance drop may be related to a possible onset of superconductivity in this particular, i.e. our least disordered, NW. Unfortunately, this superconducting transition is very broad and is not complete even down to our lowest measurement temperature of 0.3 K. Provided that this scenario is accepted, one plausible explanation would be that a full transition to a superconducting state has been hindered by the presence of a large amount of point defects in our as-grown ITO NWs, as discussed. Indeed, we notice that signatures of inherent superconductivity in ITO materials have previously been reported by several authors [25, 26]. Nevertheless, the situation is more complex in a disordered system, as the disorder effect can significantly suppress the superconducting transition. For instance, in a 87 nm thick ITO film, only a small (<1%) resistance drop was found between 3.5 and 1.5 K, which was understood in terms of a competition between electron localization and superconductivity [25]. In our case, the zero-field resistance dropped by ∼5% when the temperature was reduced from 5 to 2 K. Our resistance drop is larger likely because our ITO-g NW has a lower ρ(300 K) value of 137 $\mu\Omega$ cm, as compared with that (590 $\mu\Omega$ cm) in the 87 nm think ITO film mentioned above. Once the temperature is raised to be above 5 K, the magnetic field effect on resistance becomes negligibly small. Between 5 and 10 K, we found a negative magnetoresistance of $[\rho(B = 1\text{ T}) - \rho(0)]/\rho(0) \approx -0.001$ (not shown). This minute magnetoresistance suggests that magnetic impurities barely played a significant role in our NWs. High-quality single-crystalline NW samples with low resistivities (for example, ρ(300 K) $\lesssim$ 100 $\mu\Omega$ cm) will be very useful for addressing the superconductivity problem in ITO materials. The various behaviors that we observed in figures 5 and 6 reflect the richness and subtlety (which

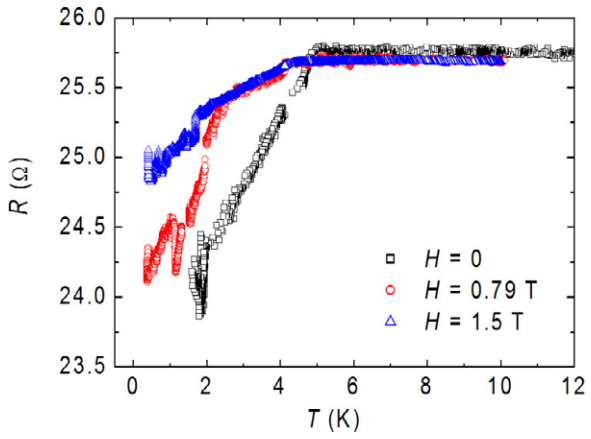

Figure 6. Resistance as a function of temperature for the ITO-g NW in zero magnetic field and in two magnetic fields of 0.79 and 1.5 T, as indicated. The magnetic fields were applied perpendicular to the direction of the current flow.

[8] By taking a value of $N(0) \approx 10^{45}$–10^{46} states J^{-1} m^{-3}, a dynamic defect concentration of $n_i \sim 10^{23}$–10^{25} m^{-3} will give rise to a relative resistivity rise of $\rho_{2CK}/\rho_{min} \sim 0.015$.

could be associated with the dynamic point defects) of the low-temperature electrical properties of ITO NWs. This issue deserves further theoretical and experimental investigations.

4. Conclusion

We have measured the intrinsic temperature behavior of resistivity for individual ITO NWs from 300 down to 1.5 K, employing the four-probe measurement configuration. Low-resistance ohmic Ti/Au electrodes were fabricated by using the electron-beam lithography technique. The overall temperature behavior of resistivity suggests that the as-grown ITO NWs are metallic, but disordered. The metallic property is well described by the Bloch–Grüneisen law. However, electron scattering off dynamic point defects causes an additional temperature-dependent correction to the resistivity at low temperatures. The dynamic defects are likely associated with the numerous point defects which inevitably exist in as-grown ITO NWs. This work demonstrates that the four-probe electrical-transport method can serve as a powerful probe for the microscopic quality of the atomic structure in a given nanoscale device.

Acknowledgments

The authors thank Sheng-Shiuan Yeh for helpful discussions. This work was supported by the Taiwan National Science Council through grant nos. NSC 95-2120-M-009-002 and NSC 97-2120-M-009-005, and by the MOE ATU Program.

References

[1] Lieber C M and Wang Z L 2007 *MRS Bull.* **32** 99
[2] Lu J G, Chang P C and Fan Z 2006 *Mater. Sci. Eng.* R **52** 49
[3] Lin J F, Bird J P, Rotkina L and Bennett P A 2003 *Appl. Phys. Lett.* **82** 802
[4] Wang H, Wang J, Tian M, Bell L, Hutchinson E, Rosario M M, Liu Y, Amma A and Mallouk T 2004 *Appl. Phys. Lett.* **84** 5171
[5] Vaurette F, Leturcq R, Nys J P, Deresmes D, Grandidier B and Stíevenard D 2008 *Appl. Phys. Lett.* **92** 242109
[6] Chang P C, Chien C J, Stichtenoth D, Ronning C and Lu J G 2007 *Appl. Phys. Lett.* **90** 113101
[7] Song S, Hong W K, Kwon S S and Lee T 2008 *Appl. Phys. Lett.* **92** 263109
[8] Rueß F J, Weber B, Goh K E J, Klochan O, Hamilton A R and Simmons M Y 2007 *Phys. Rev.* B **76** 085403
[9] Lin Y H, Sun Y C, Jian W B, Chang H M, Huang Y S and Lin J J 2008 *Nanotechnology* **19** 045711
[10] Motayed A, Davydov A V, Mohammad S N and Melngailis J 2008 *J. Appl. Phys.* **104** 024302
[11] Chiu S P, Lin Y H and Lin J J 2009 *Nanotechnology* **20** 015203
[12] Peng X S, Meng G W, Wang X F, Wang Y W, Zhang J, Liu X and Zhang L D 2002 *Chem. Mater.* **14** 4490
[13] Wan Q, Song Z T, Feng S L and Wang T H 2004 *Appl. Phys. Lett.* **85** 4759
[14] Li S Y, Lee C Y, Lin P and Tseng T Y 2005 *Nanotechnology* **16** 451
[15] Kalyanikutty K P, Gundiah G, Edem C, Govindaraj A and Rao C N R 2005 *Chem. Phys. Lett.* **408** 389
[16] Lin D, Wu H, Zhang R and Pan W 2007 *Nanotechnology* **18** 465301
[17] Li Z Q and Lin J J 2004 *J. Appl. Phys.* **96** 5918
[18] Liu X D, Jiang E Y and Zhang D X 2008 *J. Appl. Phys.* **104** 073711
[19] Lin B T, Chen Y F, Lin J J and Wu C Y 2008 in preparation
[20] Tahar R B H, Ban T, Ohya Y and Takahashi Y 1998 *J. Appl. Phys.* **83** 2631
[21] Wan Q, Dattoli E N, Fung W Y, Guo W, Chen Y, Pan X and Lu W 2006 *Nano Lett.* **6** 2909
[22] Chiquito A J, Lanfredi A J C, de Oliveira R F M, Pozzi L P and Leite E R 2007 *Nano Lett.* **7** 1439
[23] Lin Y H, Chiu S P and Lin J J 2008 *Nanotechnology* **19** 365201
[24] Larsson M W, Wallenberg L R, Persson A I and Samuelson L 2004 *Microsc. Microanal.* **10** 41
[25] Ohyama T, Okamoto M and Otsuka E 1985 *J. Phys. Soc. Japan* **54** 1041
[26] Mori N 1993 *J. Appl. Phys.* **73** 1327
[27] Ziman J M 1960 *Electrons and Phonons* (Oxford: Clarendon)
[28] Liu Y L, Wu Z Y, Lin K J, Huang J J, Chen F R, Kai J J, Lin Y H, Jian W B and Lin J J 2007 *Appl. Phys. Lett.* **90** 013105
[29] Al'tshuler B L and Aronov A G 1985 *Electron–Electron Interactions in Disordered Systems* ed A L Efros and M Pollak (Amsterdam: Elsevier)
[30] Lin J J and Wu C Y 1993 *Phys. Rev.* B **48** 5021
[31] Affleck I and Ludwig A W W 1993 *Phys. Rev.* B **48** 7297
[32] Aliev F G, Moshchalkov V V and Bruynseraede Y 1998 *Phys. Rev.* B **58** 3625
[33] Cichorek T, Sanchez A, Gegenwart P, Weickert F, Wojakowski A, Henkie Z, Auffermann G, Paschen S, Kniep R and Steglich F 2005 *Phys. Rev. Lett.* **94** 236603
[34] Mryasov O N and Freeman A J 2001 *Phys. Rev.* B **64** 233111
[35] Odaka H, Shigesato Y, Murakami T and Iwata S 2001 *Japan. J. Appl. Phys.* **40** 3231
[36] Kittel C 2005 *Introduction to Solid State Physics* (New York: Wiley)
[37] Kondo J 1964 *Prog. Theor. Phys.* **32** 37